Check for updates

Synthesis and characterisation of antimicrobial metal–organic frameworks as multi-drug carriers†

Ahmed Ahmed, [iD] [a,b] Aileen Kelly,[b] Dayle Leonard,[c] Waleed Saleem,[b] Andrey Bezrukov, [iD] [d] Constantinos G. Efthymiou,[a] Michael J. Zaworotko, [iD] [a,d] Davide Tiana, [iD] [a,e] Aoife Boyd [iD] [c] and Constantina Papatriantafyllopoulou [iD] *[a,b]

Antibiotic resistance is a significant global concern, necessitating the development of either new antibiotics or advanced delivery methods. With this in mind, we report on the synthesis and characterisation of a new family of Metal–Organic Frameworks (MOFs), **OnG6** MOFs, designed to act as multi-drug carriers for bacterial infection treatment. **OnG6** is based on the pro-drug 4,4'-azodisalicylic acid (AZDH$_4$), which *in vivo* produces two equivalents of *para*-aminosalicylic acid (ASA), a crucial drug for *M. tuberculosis* treatment. X-ray and computational studies revealed that **OnG6** MOFs are mesoporous MOFs with **etb** topology and an [M$_2$(AZD)] formula (M = Zn, **OnG6-Zn**; Mg, **OnG6-Mg**; Cu, **OnG6-Cu**; and Co, **OnG6-Co**), featuring 1-dimensional channel type pores of 25 Å diameter. **OnG6** MOFs are the first reported MOFs bearing the ligand AZDH$_4$, joining the family of mesoporous MOFs arranged in a honeycomb pattern. They absorb isoniazid (INH) and ciprofloxacin (CIPRO) with the former being a specific antibiotic for *M. tuberculosis*, and the latter being a broader-spectrum antibiotic. The stability of the MOFs and their capacity for antibiotic uptake depend on the nature of the metal ion, with **OnG6-Mg** demonstrating the highest drug absorption. The antimicrobial activity of these species was assessed against *S. aureus* and *E. coli*, revealing that the carriers containing CIPRO displayed optimal efficacy.

Introduction

Metal–organic frameworks (MOFs) are a family of crystalline porous materials that consist of inorganic building units linked through organic linkers.[1–3] They possess various desirable features, such as high porosity, large surface area, tuneable structures, and high thermal stability, which make them suitable for industrial, environmental, and biomedical applications.[4–10] In the biomedical field, MOFs have been extensively studied as contrast agents or drug carriers for anti-cancer drugs. They have also been found to provide protection to large biomolecules from degradation and release them in a controlled manner, while showing promising advancements in gene targeting, enzyme immobilisation, and protein crystallisation and purification.[7,11–13] Recently, the use of MOFs in antimicrobial applications has garnered substantial attention, particularly due to their potential to combat antibiotic resistance.[14]

Antibiotic resistance poses a significant global health threat, with an alarming projection of 10 million annual deaths by 2050 due to drug-resistant bacterial infections.[15,16] Several strategies have been implemented to prevent the development of antibiotic resistance. These, among others, include efforts to develop new classes of antibiotics. Additionally, new methods are being investigated, with a particular focus on polytherapeutic nanoparticles that can carry antibiotics to the active site within bacteria, thus bypassing any resistance caused by membrane changes or efflux pumps.[17,18] Although these approaches demonstrate potential, they also present limitations, especially regarding the stability, scalability, and targeted delivery capabilities of the nanoparticles. On the other hand, the development of new classes of antibiotics is slow and cannot keep up with the emergence of antibiotic-resistant bacteria. As a result, the creation of innovative strategies to combat antibiotic resistance remains essential.

MOFs are uniquely positioned to address antibiotic resistance as their high porosity and tunability enable them to interact with bacteria in multiple ways.[14,19,20–23] Besides

[a]*SSPC The Science Foundation Ireland Research Centre for Pharmaceuticals, Ireland*
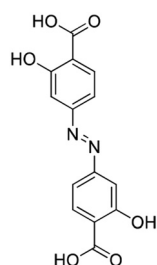[b]*School of Biological and Chemical Sciences, College of Science and Engineering, University of Galway, H91 TK 33 Galway, Ireland. E-mail: constantina.papatriantafyllopo@universityofgalway.ie; Tel: +353 91 493462*
[c]*School of Natural Sciences, College of Science and Engineering, University of Galway, H91 TK 33 Galway, Ireland*
[d]*Department of Chemical Sciences, Bernal Institute, University of Limerick, Limerick, V94T9PX, Republic of Ireland*
[e]*School of Chemistry, University College Cork, College Road, Cork, Ireland*
†Electronic supplementary information (ESI) available: Additional details of crystallography, spectroscopy, encapsulation, and cytotoxicity data. See DOI: https://doi.org/10.1039/d4dt01100g
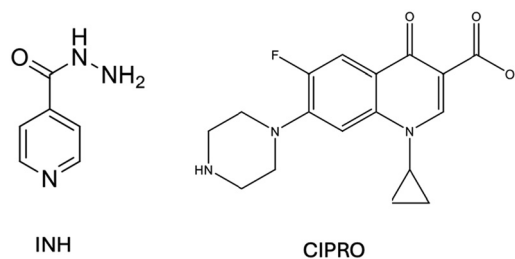
serving as drug carriers for antibiotics, they can exhibit inherent antimicrobial properties when they contain bactericidal metals or linkers. Currently, several MOFs with antibacterial properties are known. In particular, MOFs that can encapsulate antimicrobial species, such as antibiotics, metals, metal oxides, and enzymes, and release them in a controlled manner have been reported.[19,20] Among them, **ZIF-8** demonstrates an excellent ability to absorb a variety of different antibiotics, including ceftazidime, gentamicin, ciprofloxacin, and rifampicin.[21] Furthermore, most Ag^+ MOFs show intrinsic antibacterial activity, while there are MOFs that are composed of bactericidal metals and linkers, releasing both for an increased therapeutic effect.[22] A representative example of this is **BioMIL-5**, which shows bacteriostatic effects over 7 days at concentrations as low as 0.9 mg mL^{-1}.[23a] Yet, this field is still in its infancy, and the isolation of MOFs that incorporate more than two mechanisms of action is currently limited. The latter could offer significant opportunities to develop more efficient treatments for bacterial infections.

With the above in mind, we decided to explore the use of the ligand 4,4′-azodisalicylic acid (AZDH$_4$, Scheme 1) for synthesising MOFs with multi-drug antibacterial action. AZDH$_4$ is reduced *in vivo* by bacterial or mammalian azoreductases, resulting in two equivalents of active *para*-aminosalicylic acid (ASA).[24] ASA acts by inhibiting the biosynthesis of folate in *M. tuberculosis*. Moreover, the incorporation of different metal ions in the MOF SBU, coupled with the encapsulation of extra antibiotics within its pores, could potentially create multi-action antibacterial materials. The latter may benefit from the toxicity of metal ions and the combined action of two distinct antibacterial agents. In addition, there could also be a synergistic effect of the three, resulting in advanced materials with at least three different mechanisms of antibacterial action.

Herein, we report on the synthesis and characterisation of a new family of MOFs with the formula [M$_2$(AZD)] (M = Zn, **OnG6-Zn**; Mg, **OnG6-Mg**; Cu, **OnG6-Cu**; and Co, **OnG6-Co**). **OnG6** MOFs are mesoporous with an **etb** topology. They are the first MOFs containing the ligand AZDH$_4$ in either its neutral or ionic form, being new additions to the limited group of mesoporous MOFs in a honeycomb topology.[25] **OnG6** can absorb antibiotics, including isoniazid (INH) and ciprofloxacin (CIPRO), Scheme 2. The antimicrobial activity of these carriers was tested against *S. aureus* and *E. coli*. It was found

Scheme 2 Schematic representation of isoniazid (INH) and ciprofloxacin (CIPRO).

that the carriers loaded with CIPRO displayed optimal efficacy with the **OnG6-Mg** analogue having one of the highest bioactive compound uptake among MOFs.[23,26]

Experimental

All chemicals used were commercially available and used without further purification. All procedures were conducted under aerobic conditions unless stated otherwise.

Synthesis of 4,4′-azodisalicylic acid (AZDH$_4$)

4-Nitrosalicylic acid (1.5 g, 8.2 mmol) was added to a 5M aqueous NaOH solution (22.5 mL) in a 250 mL conical flask, resulting in a dark red solution. The solution was stirred at 50 °C in open air. In a separate conical flask, D-(+)-glucose (10 g, 55 mmol) was dissolved in H$_2$O (10 mL) by heating to 50 °C. The glucose solution was slowly added to the 4-nitrosalicylic acid solution, yielding a black solution. The latter was stirred for 15 minutes at 50 °C, then cooled to room temperature and stirred for two days in open air. After two days, a dark brown suspension formed. The suspension was acidified to pH 1 using concentrated HCl and then filtered, yielding a dark brown precipitate. This precipitate was washed with excess H$_2$O and dried at 60 °C overnight. The crude product was recrystallised from a boiling saturated Na$_2$CO$_3$ solution, producing bright orange Na$_4$AZD needles. The crystals were collected by filtration and dried overnight at 60 °C. Then, they were redissolved in a minimal amount of H$_2$O and acidified to pH 1 using concentrated HCl, resulting in an orange precipitate. This precipitate was collected by filtration, washed with excess water, and dried overnight at 60 °C. Yield: 68%; ^{1}H-NMR (500 MHz, DMSO-d$_6$) δ 7.395 (d, 2H), δ 7.422 (dd, 2H), δ 7.987 (d, 2H) ^{13}C-NMR: (500 MHz, DMSO-d$_6$) δ 111.50, δ 113.75, δ 116.25, δ 131.75, δ 156.25, δ 162.20, δ 171.57. HRMS (ESI/Q-TOF) m/z: [M + HCOO$^-$] calculated for C$_{14}$H$_8$N$_2$O$_6$ = 345.0359, found = 345.0344. IR (ν, cm^{-1}): 1653(s), 1610(m), 1572(m), 1484(w), 1428(s), 1364(w), 1286(m), 1206(s), 1149(m), 1090(w), 977(m), 882(m), 783(s), 742(m), 631(m).

Synthesis of [Zn$_2$(AZD)] (OnG6-Zn)

AZDH$_4$ (30 mg, 0.1 mmol) was dissolved in DMF (5 mL) in a glass scintillation vial. The solution was sonicated for

Scheme 1 Schematic representation of 4,4′-azodisalicylic acid (AZDH$_4$).

2 minutes. $Zn(NO_3)_2·6H_2O$ (119 mg, 0.4 mmol) was added and the solution was sonicated for a further 3 minutes. The vial was capped and placed in an oven at 100 °C for 6 hours, yielding red microcrystalline spheroids of **OnG6-Zn**. The solvent was then decanted and the crystals were washed with excess DMF. Yield: 67%. Anal. calcd (found) for **OnG6-Zn**: C, 35.59 (35.82%); H, 1.49 (1.74%); N, 6.92 (7.01%). IR (ν, cm^{-1}): 1595(w), 1564(m), 1495(w), 1420(s), 1376(m), 1315(w), 1231(m), 1145(w), 1016(w), 989(m), 879(w), 840(w), 790(m), 751(m), 699(w).

Synthesis of [Mg₂(AZD)] (OnG6-Mg)

$AZDH_4$ (30 mg, 0.1 mmol) was dissolved in DMF (4 mL) in a glass scintillation vial. Then, EtOH (1 mL) and H_2O (1 mL) were added, and the solution was sonicated for 3 minutes. $Mg(NO_3)_2·6H_2O$ (77 mg, 0.3 mmol) was then added and the solution was sonicated for a further 3 minutes. The vial was capped and placed in an oven at 100 °C for 24 hours, yielding red microcrystalline spheroids of **OnG6-Mg**. The solvent was decanted and the crystals were washed with excess DMF. Yield: 53%. Anal. calcd (found) for **OnG6-Mg**: C, 44.65 (44.91%); H, 1.87 (2.04%); N, 8.68 (8.83%). IR (ν, cm^{-1}): 1656(s), 1602(w), 1577(m), 1498(w), 1436(s), 1382(s), 1317(m), 1251(s), 1138(w), 1097(m), 989(m), 891(w), 840(m), 796(m), 754(m), 713(w), 680(w), 659(m).

Synthesis of [Cu₂(AZD)] (OnG6-Cu)

$AZDH_4$ (30 mg, 0.1 mmol) was dissolved in DMF (4 mL) in a glass scintillation vial. EtOH (0.5 mL) and H_2O (1.5 mL) were added. The solution was sonicated for 2 minutes, after which, $Cu(NO_3)_2·5H_2O$ (93 mg, 0.4 mmol) was added. The solution was sonicated for 3 minutes. The vial was capped and placed in an oven at 100 °C for 24 hours, yielding green microcrystalline spheroids of **OnG6-Cu**. The solvent was decanted and the crystals were washed with excess DMF. Yield: 36%. Anal. calcd (found) for **OnG6-Cu**: C, 35.92 (36.17%); H, 1.51 (1.87%); N, 6.98 (7.22%). IR (ν, cm^{-1}): 1599(m), 1558(m), 1497(m), 1439(s), 1378(w), 1308(m), 1242(m), 1141(w), 991(m), 886(w), 784(m), 752(m), 679(w).

Synthesis of [Co₂(AZD)] (OnG6-Co)

$AZDH_4$ (30 mg, 0.1 mmol) was dissolved in DMF (5 mL) in a glass scintillation vial. The solution was sonicated for 2 minutes. $Co(NO_3)_2·6H_2O$ (29 mg, 0.1 mmol) was added to the solution, after which the solution was sonicated for a further 3 minutes. The vial was then sealed and placed in an oven at 105 °C for 24 hours, yielding purple microcrystalline spheroids of **OnG6-Co**. The solvent was decanted and the crystals were washed with excess DMF. Yield: 61%. Anal. calcd (found) for **OnG6-Co**: C, 36.76 (37.19%); H, 1.54 (1.42%); N, 7.15 (6.81%). IR (ν, cm^{-1}): 1567(m), 1423(s), 1373(m), 1299(m), 1236(m), 1142(w), 1043(w), 989(w), 790(m), 753(m), 702(w).

Physical studies

FTIR spectra (4000–400 cm^{-1}) were recorded using a PerkinElmer 16PC FT-IR spectrometer with samples prepared as KBr pellets. HRM was carried out on a Waters LCT instrument using ESI time-of-flight mass spectrometry in negative mode. SEM images of the frameworks were collected on a Hitachi S-4700 SEM. A 5 kV electron beam was used for imaging, whilst a 20 kV electron beam was used for EDX analysis. Samples were sputtered with gold prior to SEM/EDX analysis.

PXRD data collection and analysis

Diffractograms were recorded using a PANalytical Empyrean™ diffractometer equipped with a PIXcel 3D detector operating in scanning line detector mode with an active length of 4 utilizing 255 channels. The diffractometer is equipped with an Empyrean Cu LFF (long fine-focus) HR (9430 033 7310x) tube operated at 40 kV and 40 mA. CuKα radiation (λ_α = 1.540598 Å) was used for diffraction experiments. Continuous scanning mode with the goniometer in the theta–theta orientation was used to collect the data. Incident beam optics included the fixed divergence slit with the anti-scatter slit PreFIX module, with a 1/8° divergence slit and a 1/4° anti-scatter slit, as well as a 10 mm fixed incident beam mask and a Soller slit (0.04 rad). Divergent beam optics included a P7.5 anti-scatter slit, a Soller slit (0.04 rad), and a Ni-β filter. In a typical experiment, 20 mg of sample was dried in air, ground into a fine powder and loaded on a zero background silicon disk. Data were collected in the 2θ range of 2.8°–40° with a step-size of 0.026° and a scan time of 200 seconds per step.

Unit cell parameters of the frameworks were determined from the powder X-ray diffraction pattern. Initial unit cell parameters for the frameworks were determined from positions of 10 observed peaks using indexing *via* DICVOL[27] implemented in DASH.[28] The found unit cell parameters were refined for all frameworks *via* Pawley profile fit of the powder X-ray diffraction pattern using GSAS-II (Fig. S1–S4 in the ESI†).[29]

Crystal structure model construction

All calculations were performed using the open-source software Quantum Espresso v7.1 at the PBEsol level of theory.[30] Norm conserving pseudopotentials were used with an energy cut-off of 110 Ry. The unit cell parameters for the **OnG6** MOFs display significant similarities to those of the M_2(olsalazine) MOFs (Table S1†), where olsalazine is an isomer of $AZDH_4$.[26] Based on this, the initial structure was derived from M_2(olsalazine), with modifications made by changing the organic ligand from olsalazine to $AZDH_4$. A full geometry optimization was then performed on the primitive cell of the MOF relaxing both the atomic positions and the lattice parameters. The standard convergence parameters were adopted.

Dissolution studies

A sample of MOF (5 mg) was suspended in a deionised water and PBS solution (pH 7.4, 15 mL) in a centrifuge vial, which was then maintained at 37 °C and stirred. The vials were periodically centrifuged at 4500 rpm for 5 minutes. After each centrifugation, 500 μL aliquots of the supernatant were taken

and diluted to 5 mL with deionised water. The release was monitored using UV-Vis spectroscopy.

MOF activation and drug loading

A sample of MOF (20 mg) was placed in a two-neck round bottom flask. One neck was sealed with a septum, while the other was attached to a vacuum pump. The sample was then vacuumed, and the flask was placed in an oil bath at 180 °C. In a single neck round bottom flask, the drug (INH or CIPRO, 50 mg) was added, and the flask was sealed with a septum. The flask was then purged with N_2 for 10 minutes using a balloon, after which dry EtOH (15 mL) was introduced *via* a syringe. This solution was sonicated to dissolve the drug. After 8 hours, the MOF sample was allowed to cool to room temperature under vacuum. N_2 was then introduced to the system using a balloon and needle. The vacuum was then removed, and the flask was stoppered. Finally, the drug solution was added using a syringe, and the MOF sample was left in the solution for 3 days.

Quantification of drug loading by ^{1}H-NMR

15 mg of drug loaded MOF material was suspended in DMSO-d_6 (500 μL) and 25 μL of DCl (35 wt% in D_2O). The suspension was sonicated for 5 minutes yielding a clear solution. ^{1}H-NMR spectra were recorded at 500 MHz using a Bruker spectrometer and were processed using Bruker TopSpin software with calibration against solvent signals in the literature.

Minimum inhibitory concentration assay

Antimicrobial activity was quantified using the broth dilution method as previously described.[31] Cultures of Gram-positive *Staphylococcus aureus* (8325-4)[32] and Gram-negative enterotoxigenic *Escherichia coli* (ETEC) DSMZ 10973 (DSMZ) were inoculated at OD_{600} = 0.001 [equivalent to 1×10^6 Colony Forming Units (CFU) mL^{-1}] in 96-well microtitre plates in brain heart infusion broth (Oxoid) containing 2-fold serially diluted MOF or pure antibiotics (INH and CIPRO). For initial assessment a concentration range of 1000–8 μg ml^{-1} MOFs was used. MOFs with MIC < 8 μg ml^{-1} were further analysed at concentrations of 31–0.2 μg ml^{-1} and/or 1.7–0.01 μg ml^{-1}. Control samples contained only bacteria, while blank samples contained only media. The samples were incubated for 16–18 h at 37 °C and the absorbance at 600 nm was measured using a Tecan microplate reader with Magellan software. Experiments were conducted at least twice in triplicate.
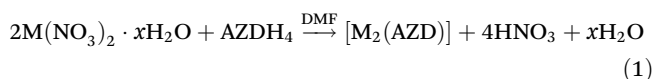
Results and discussion

Synthesis

Our group has been investigating the synthesis and characterisation of new MOFs with drug carrier properties. This endeavour has led to the development of the **NUIG** family of MOFs, notable for their exceptional uptake of drugs like nitric oxide, ibuprofen, and doxorubicin.[6,8] To broaden the scope of our research, and with an aim to develop MOFs capable of carrying

multiple antibacterial drugs, we have now turned our attention to the utilisation of the ligand $AZDH_4$ in the synthesis of MOFs. A schematic representation of $AZDH_4$ synthesis is shown in Scheme 3.

Several reaction conditions and synthetic parameters, such as the molar ratio of the reactants, solvents, metal sources, and temperature, were investigated, and much effort was made to improve the crystallinity of the products. The reaction between $AZDH_4$ and an excess of a nitrate metal salt in DMF at high temperature provided access to the **OnG6** family of MOFs with the formula $[M_2(AZD)]$, where M = Mg, **OnG6-Mg**; Zn, **OnG6-Zn**; Cu, **OnG6-Cu**; and Co, **OnG6-Co**. The stoichiometric equation that describes the synthesis of the **OnG6** MOFs is shown in eqn (1).
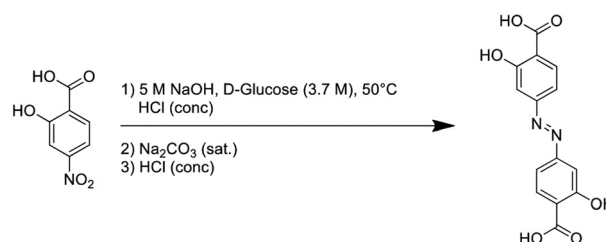
$$2M(NO_3)_2 \cdot xH_2O + AZDH_4 \xrightarrow{DMF} [M_2(AZD)] + 4HNO_3 + xH_2O \quad (1)$$

OnG6

Preliminary characterisation of the **OnG6** MOFs was conducted using IR spectroscopy. Several bands appear in the 1655–1360 cm^{-1} region in the IR spectra of all **OnG6** analogues (Fig. S5†), confirming the coordination of the $AZDH_4$ linker. This region would typically exhibit contributions from carboxylate $\nu_{as}(CO_2)$ and $\nu_s(CO_2)$ modes. However, overlap with the stretching vibrations of the aromatic ring makes detailed assignment difficult.

Description of structures

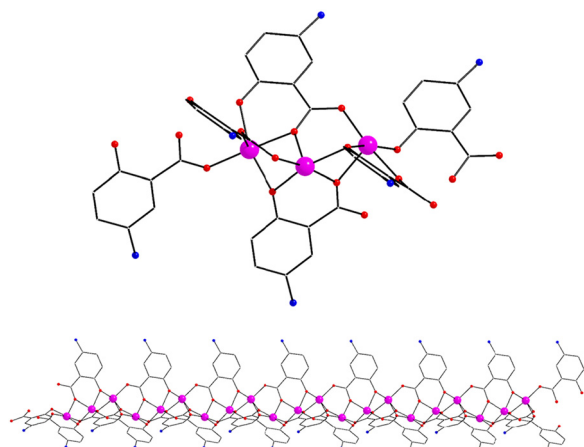Representation of the molecular structure of **OnG6** is shown in Fig. 1 and 2.

OnG6 MOFs crystallise in a hexagonal crystal system. They adopt an **etb** network, based on rod-shaped SBUs with the formula $[M_3(AZD)_{1.5}]$ or $[M_3(-RO)_3(-RCO_2)_3]$, where $-RO^-$ and $-RCO_2^-$ are alkoxy and carboxylate groups coming from three AZD^{4-} ligands (Fig. 1). The latter bridge the neighbouring building units, resulting in the formation of hexagonal tubes, which are further linked, creating a three-dimensional network in a honeycomb arrangement (Fig. 1). Consequently, **OnG6** MOFs feature hexagonal 1-D channel type pores. The frameworks are mesoporous with pores approximately 25 Å in diameter. The coordination mode of the AZD^{4-} ligand in the **OnG6** MOFs is depicted in Scheme 4.
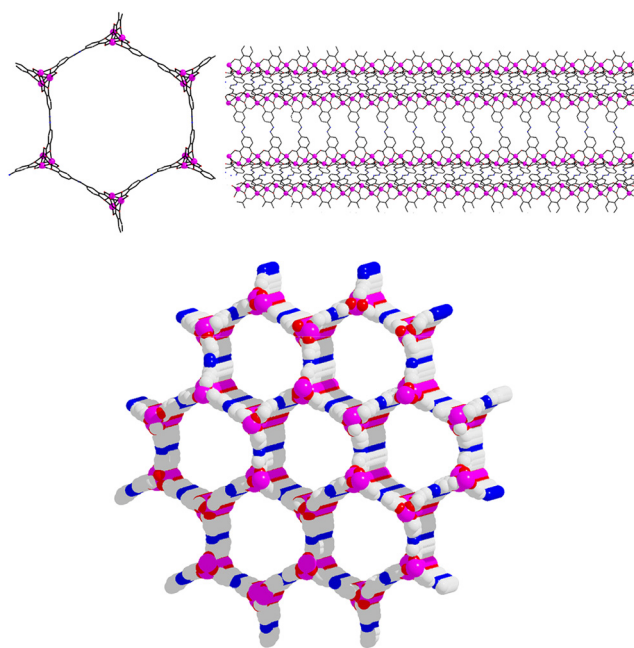

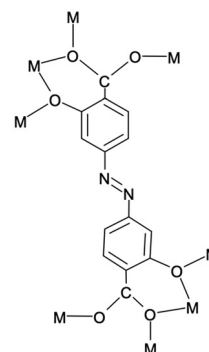Scheme 3   Schematic representation of the $AZDH_4$ synthesis.

Fig. 1 Representation of the trinuclear repeating unit (top) of the rod SBU (bottom) in **OnG6** MOFs. Colour code: N, dark blue; M, purple (Mg, **OnG6-Mg**; Zn, **OnG6-Zn**; Cu, **OnG6-Cu**; and Co, **OnG6-Co**); O, red; and C, grey.
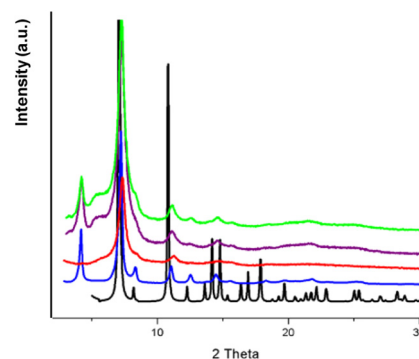

Fig. 2 Representation of the hexagonal tube along *c* and *a* axes (top left and top right, respectively) in **OnG6** MOFs, and a space-filling representation of the three dimensional network in a honeycomb arrangement (bottom). Colour code: N, dark blue; M, purple (Mg, **OnG6-Mg**; Zn, **OnG6-Zn**; Cu, **OnG6-Cu**; and Co, **OnG6-Co**); O, red; and C, grey.

OnG6 MOFs were further characterised by PXRD and SEM analyses. The experimental PXRD patterns of **OnG6** MOFs were compared with the one calculated from simulation confirming the proposed MOF crystal structures (Fig. 3).
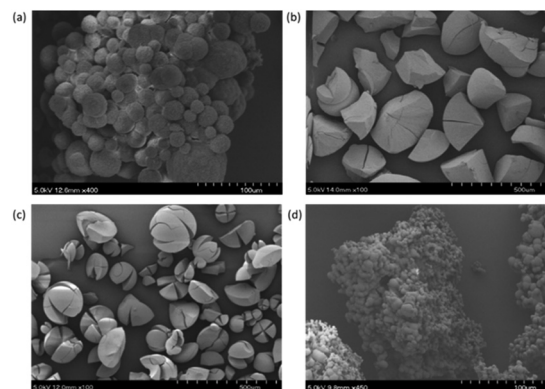
The SEM images of the **OnG6** particles reveal a spheroid morphology with a wide range of particle sizes (Fig. 4). Upon further magnification, the spheroids are found to be composed of needle-shaped crystallites. The size of carriers,

Scheme 4 A schematic representation of the coordination mode AZD^{4-} in the **OnG6** MOFs, bridging eight metal ions.

Fig. 3 Experimental PXRD patterns of the **OnG6** MOFs in comparison with the one derived from the computational model. Colour code: model, black; **OnG6-Zn**, blue; **OnG6-Mg**, red; **OnG6-Co**, purple; and **OnG6-Cu**, green.

Fig. 4 SEM images of (a) **OnG6-Cu**, (b) **OnG6-Zn**, (c) **OnG6-Mg** and (d) **OnG6-Co**.

especially those for antibiotic delivery, is crucial in developing effective pulmonary drug delivery systems with MOF particles with an aerodynamic diameter between 0.5 and 5 μm being suitable for pulmonary delivery through inhalation as powders.[33] Inhalable drug carriers are proposed to treat pulmonary *M. tuberculosis* as they serve as an alternative to orally

administered drugs, aiming to overcome the latter's barriers in reaching the site of action. Interestingly, **OnG6-Cu** and **OnG6-Co** particles are the closest to the optimum size for pulmonary delivery by inhalation with average particle sizes of 28 and 10 μm, respectively.

Dissolution and drug uptake studies

Framework dissolution studies were carried out in water and PBS solution (pH 7.4) at 37 °C to determine the rate of linker release (Fig. 5). The release was monitored using UV-Vis spectroscopy at λ = 325 nm. A calibration curve of $Na_4(AZD)$ in water was used to quantify AZD^{4-} concentration (Fig. S6†). Due to the high biocompatibility of Mg^{2+}, Zn^{2+} and Cu^{2+}, **OnG6-Mg**, **OnG6-Zn** and **OnG6-Cu** were prioritised for dissolution studies. Further to their biocompatibility, these MOFs exhibit the highest bioactive compound loadings among all MOFs, with **OnG6-Mg** comprising 85% AZD^{4-}.[23,26] UV-Vis data for framework dissolution for the three MOFs are illustrated in Fig. S7–S9 in the ESI.†

The dissolution curves in water clearly show the effects of different metals on the water stability of the frameworks. **OnG6-Mg** breaks down rapidly, releasing 63% of AZD^{4-} within 10 minutes. **OnG6-Zn** is more stable, releasing 29% of the linker after 30 minutes. The **OnG6-Cu** framework is the most stable, releasing only 21% of the linker after 5 hours. A similar pattern is observed in PBS, where **OnG6-Mg** and **OnG6-Zn** break down within 10 minutes. **OnG6-Cu** demonstrates significant stability, with only 42% of AZD^{4-} released after 2 days.

Given the enhanced porosity of the **OnG6** MOFs and the need for multi-drug delivery in the treatment of drug-resistant bacterial infections, the capability of **OnG6** to encapsulate the antitubercular drug, isoniazid (INH), was examined. To access the full porosity of the frameworks, they were activated prior to INH loading. The loading of INH was performed under a N_2 atmosphere immediately after activation. A MOF sample was suspended in a solution of INH in dry ethanol. The INH@**OnG6** species were collected by centrifugation and washed thoroughly with EtOH to remove any INH on the surface. The loading was quantified by ^{1}H-NMR after the framework was digested in DCl/DMSO-d^6. The ^{1}H-NMR spectra of AZDH$_4$, INH, and INH@**OnG6** are shown in Fig. S10–S13 in the ESI.† INH signals (doublet, 2H) at 9.12 ppm and AZDH$_4$ signals (doublet, 2H) at 7.98 ppm were integrated for INH loading quantification.

The INH loadings for **OnG6-Zn** and **OnG6-Mg** are presented in Table S2,† along with the relative stoichiometry derived from the ^{1}H-NMR studies. **OnG6-Zn** shows a low loading of only 4 wt%. This could be a result of incomplete activation or partial framework collapse. Many **Zn-MOF-74** analogues exhibit similar behaviour, with Zn^{2+} analogues being the least stable in terms of activation.[26,34] Conversely, **OnG6-Mg** loads significantly more INH (22 wt%), likely because of its higher stability. **OnG6-Cu** turned black when heated, suggesting its collapse, which subsequently impeded INH absorption.

INH is specifically used for *M. tuberculosis* treatment, and in order to gain a better insight into the antimicrobial activity of **OnG6** MOFs, the investigation of a broader-spectrum antibiotic was targeted. To this end, ciprofloxacin was chosen;[35] besides its use in treating and preventing *M. tuberculosis*, this fluoroquinolone is effective against both Gram-positive and Gram-negative bacteria, making it ideal for antibacterial assays. The encapsulation method used for INH was similarly applied to CIPRO. A distinct proton signal at 8.63 ppm for CIPRO serves as a reference point. This signal appears in all CIPRO-loaded analogues, including CIPRO@**OnG6-Zn**, CIPRO@**OnG6-Mg**, and CIPRO@**OnG6-Co**, indicating a similar drug loading for the **OnG6** MOFs (Fig. 6 and Fig. S14, S15†).

Minimum inhibitory concentration studies

To investigate the antimicrobial properties of the **OnG6** MOF family, Minimum Inhibitory Concentration (MIC) studies were performed. The assays were conducted against two bacterial species: Gram-positive *S. aureus* and Gram-negative *E. coli*.[33] These strains were selected because they are well-studied model organisms with established biochemistry.[36] As common pathogenic bacteria, they pose significant health risks, making them apt candidates for antibacterial activity testing. The results of these assays can provide a general understanding of the antibacterial activity of the **OnG6** MOFs, paving the way for further investigation with more specific and highly infectious bacteria, such as *M. tuberculosis*.

The bacterial cells were incubated in brain heart infusion broth media for 16–18 hours at 37 °C, in the presence of the following materials **OnG6-Mg**, **OnG6-Zn**, **OnG6-Co**, INH, CIPRO, AZDH$_4$, INH@**OnG6-Mg**, INH@**OnG6-Zn**, CIPRO@**OnG6-Mg**, CIPRO@**OnG6-Zn**, and CIPRO@**OnG6-Co**. The MIC was determined as the minimum concentration of the compound that led to the complete inhibition of the visual growth of bacteria (Table 1).

From Table 1, it can be observed that the **OnG6** MOFs show low antimicrobial activity against both *E. coli* and *S. aureus*, with MIC values exceeding 1000 μg mL^{-1}. Similarly, INH and AZDH$_4$ show little to no inhibition, when used individually, or when formulated in the **OnG6** MOFs. This is unsurprising as both antibiotics are used almost exclusively to treat *M. tuberculosis* infections. ASA works by inhibition of folate within *M. tuberculosis* cells, whilst INH interferes with *M. tuberculosis* cell wall synthesis.[37] However, when CIPRO, a wider spectrum antibiotic, is used, a significant increase in antimicrobial activity is observed. In particular,
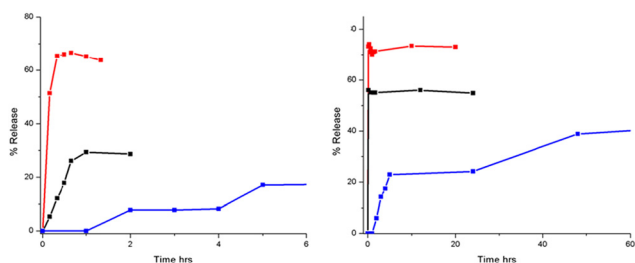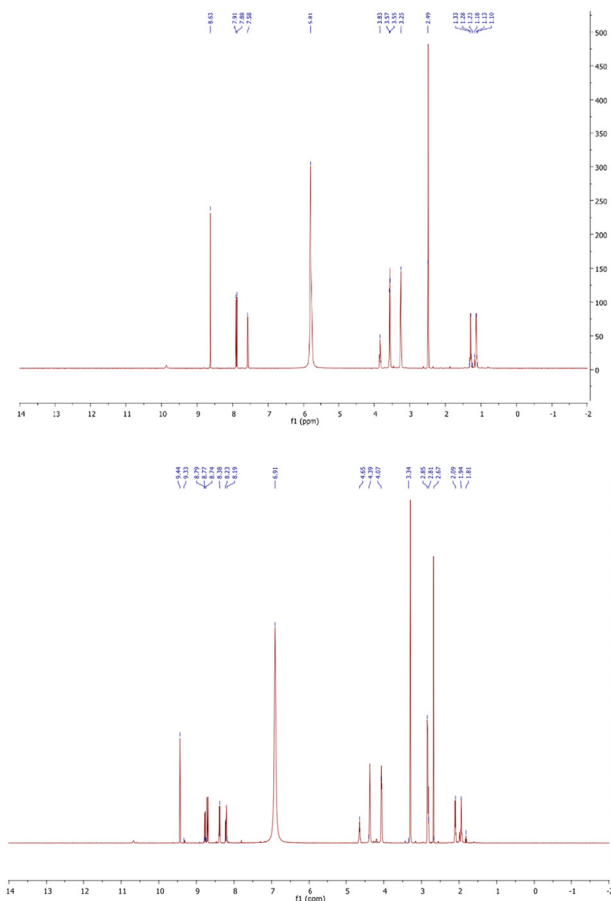

Fig. 5 **OnG6** dissolution curves in water (left) and PBS solution (right). Colour code: **OnG6-Zn**, black; **OnG6-Mg**, red; and **OnG6-Cu**, blue.

Fig. 6 Top: ^{1}H-NMR of CIPRO in DMSO-d_6/DCl. Bottom: ^{1}H-NMR of digested **OnG6-Zn** after CIPRO loading (3 days) in DMSO-d_6/DCl.

Table 1 Minimum inhibitory concentrations (µg ml^{-1}) of AZDH$_4$, INH, CIPRO, **OnG6**, INH@**OnG6**, and CIPRO@**OnG6**

Compound	Escherichia coli	Staphylococcus aureus
AZDH$_4$	>1000	500
OnG6-Co	>1000	>1000
OnG6-Mg	>1000	>1000
OnG6-Zn	>1000	>1000
INH	125	250
INH@**OnG6-Mg**	>1000	>1000
INH@**OnG6-Zn**	>1000	>1000
CIPRO	<0.01	0.05
CIPRO@**OnG6-Co**	0.1	1.9
CIPRO@**OnG6-Mg**	0.4	1.9
CIPRO@**OnG6-Zn**	0.1	0.5

CIPRO@**OnG6-Co** and CIPRO@**OnG6-Zn** exhibit strong antimicrobial activity against both bacterial strains with MIC values as low as 0.1 µg mL^{-1} for *E. coli*. Although INH, AZDH$_4$, and **OnG6** carriers showed no reactivity against the evaluated bacterial strains, the effectiveness of CIPRO and CIPRO@**OnG6** supports the hypothesis that the apparent lack of response is due to the highly specific nature of the antitubercular agents. Therefore, targeted studies against *M. tuberculosis* bacteria are necessary to establish their potential.

Conclusions

The initial employment of 4,4′-azodisalicylic acid (AZDH$_4$) in MOF chemistry led to the synthesis and characterisation of a family of mesoporous MOFs with the formula [M$_2$(AZD)], where (M = Zn, **OnG6-Zn**; Mg, **OnG6-Mg**; Cu, **OnG6-Cu**; and Co, **OnG6-Co**). **OnG6** MOFs feature an **etb** framework topology and 1-dimensional channel type pores of 25 Å diameter. **OnG6** MOFs are the first coordination compounds bearing this ligand in its neutral or ionic form.

The AZDH$_4$ linker is a prodrug of the antibiotic *para*-aminosalicylic acid (ASA), used to treat tuberculosis. The stability of the frameworks and, consequently, the release of the bioactive linker were greatly influenced by the choice of metal. **OnG6-Co** and **OnG6-Cu** display particles that are close to the optimum size for pulmonary delivery.[33] The capacity of **OnG6** for drug uptake was investigated using the antitubercular drug isoniazid (INH) and the broader-spectrum antibiotic ciprofloxacin (CIPRO). The uptake capacity of the **OnG6** analogues differs, with **OnG6-Mg** displaying the highest absorption (22 wt%). The latter also represents one of the highest bioactive compound loadings among MOFs at 88.5 wt%.[23,26]

INH, AZDH$_4$, and **OnG6** MOFs showed little to no activity against *S. aureus* and *E. coli* bacteria. Interestingly, CIPRO and CIPRO@**OnG6** exhibited good efficacy. Despite the apparent inactivity of INH, AZDH$_4$, and **OnG6** carriers against the tested bacterial strains, the effectiveness of CIPRO and CIPRO@**OnG6** indicates that the inactivity is due to the specific nature of *M. tuberculosis* and the subsequent specificity of the antitubercular agents. Studies on *M. tuberculosis* bacteria will provide further insight into the bacterial infection treatment potential of these species.

Investigation is currently underway to further reduce the MOF particle size, allowing for the study of their aerosolisation and suitability for pulmonary delivery. In addition, the isolation of mixed metal **OnG6** analogues has been targeted. This offers the opportunity to manipulate key characteristics such as water stability, linker release, biocompatibility, and antibacterial properties by selecting the appropriate metal combination.

Data availability

The data supporting this article have been included as part of the ESI.†

Conflicts of interest

There are no conflicts to declare.

Acknowledgements

References

1 (a) H.-C. J. Zhou and S. Kitagawa, *Chem. Soc. Rev.*, 2014, **43**, 5415; (b) M. Eddaoudi, D. B. Moler, H. Li, B. Chen, T. M. Reineke, M. O'Keeffe and O. Yaghi, *Acc. Chem. Res.*, 2001, **34**, 319.

2 (a) H. Furukawa, K. E. Cordova, M. O'Keeffe and O. M. Yaghi, *Science*, 2013, **341**, 1230444; (b) A. Schneemann, V. Bon, I. Schwedler, I. Senkovska, S. Kaskel and A. R. Fischer, *Chem. Soc. Rev.*, 2014, **43**, 6062.

3 (a) V. F. Yusuf, N. I. Malek and S. K. Kumar, *ACS Omega*, 2022, **49**, 44507; (b) S. Yuan, L. Feng, K. Wang, J. Pang, M. Bosch, C. Lollar, Y. Sun, J. Qin, X. Yang, P. Zhang, Q. Wang, L. Zou, Y. Zhang, L. Zhang, Y. Fang, J. Li and H.-C. Zhou, *Adv. Mater.*, 2018, **37**, 1704303.

4 N. L. Rosi, J. Eckert, M. Eddaoudi, D. T. Vodak, J. Kim, M. O'Keeffe and O. Yaghi, *Science*, 2003, **300**, 1127.

5 M. Kurmoo, *Chem. Soc. Rev.*, 2009, **38**, 1353.

6 A. Ahmed, C. G. Efthymiou, R. Sanii, E. Patyk-Kazmierczak, A. M. Alsharabasy, M. Winterlich, N. Kumar, D. Sensharma, W. Tong, S. Guerin, P. Farras, S. Hudson, D. Thompson, M. J. Zaworotko, A. J. Tasiopoulos and C. Papatriantafyllopoulou, *J. Mater. Chem. B*, 2022, **10**, 1378.

7 A. Ahmed, D. McHugh and C. Papatriantafyllopoulou, *Molecules*, 2022, **27**, 6585.

8 M. Winterlich, C. G. Efthymiou, W. Papawassiliou, J. P. Carvalho, A. J. Pell, J. Mayans, A. Escuer, M. P. Carty, P. McArdle, E. Tylianakis, L. Morrison, G. Froudakis and C. Papatriantafyllopoulou, *Mater. Adv.*, 2020, **1**, 2248.

9 J. Lee, O. K. Farha, J. Roberts, K. A. Scheidt, S. T. Nguyen and J. T. Hupp, *Chem. Soc. Rev.*, 2009, **38**, 1450.

10 P. Kumar, A. Deep and K.-H. Kim, *TrAC, Trends Anal. Chem.*, 2015, **73**, 39.

11 (a) Y. He, D. Li, L. Wu, X. Yin, X. Zhang, L. H. Patterson and J. Zhang, *Adv. Funct. Mater.*, 2023, **12**, 2212277; (b) A. Poddar, S. Pyreddy, F. Carraro, S. Dhakal, A. Russell, M. R. Field, T. S. Reddy, P. Falcaro, C. M. Doherty and R. Shukla, *Chem. Commun.*, 2020, 15406; (c) A. Ringaci, A. V. Yaremenko, K. G. Shevchenko, S. D. Zvereva and M. P. Nikitin, *Chem. Eng. J.*, 2021, **418**, 129386.

12 (a) X. Wang, P. C. Lan and S. Ma, *ACS Cent. Sci.*, 2020, **9**, 1497; (b) H. Xia, N. Li, X. Zhong and Y. Jiang, *Front. Bioeng. Biotechnol.*, 2020, 695; (c) X. Liu, W. Qi, Y. Wang, R. Su and Z. He, *Nanoscale*, 2017, **9**, 17561; (d) A. R. M. Silva, J. Y. N. H. Alexandre, J. E. S. Souza, J. G. L. Neto, P. G. De Souza Junior, M. V. P. Rocha and J. C. S. Dos Santos, *Molecules*, 2022, **27**(14), 4529.

13 (a) X. Zhang, Z. Xu, J. Zhou, X. Xing and L. Li, *Crystals*, 2022, **12**(5), 578; (b) X. Zhou, Z. Zhong, N. Xu and S. Zhong, *Crystals*, 2023, **13**, 1229; (c) J. P. Leite, D. Rodrigues, S. Ferreira, F. Figueira, F. A. Almeida Paz and L. Gales, *Cryst. Growth Des.*, 2019, **19**, 1610.

14 (a) V. Andre, A. R. F. Da Siva, A. Fernandes, R. Frade, C. Garcia, P. Rijo, A. M. M. Antunes, J. Rocha and M. T. Duarte, *ACS Appl. Bio Mater.*, 2019, **2**, 2347; (b) S. A. Ahmed, M. N. Hasan, D. Bagchi, H. M. Altass, M. Morad, I. I. Althagafi, A. M. Hameed, A. Sayqal, A. R. S. Khder, B. H. Asghar, H. A. Katouah and S. K. Pal, *R. Soc. Open Sci.*, 2020, **7**(12), 200959.

15 (a) C. L. Ventola, *P T.*, 2015, **40**(4), 277; (b) N. Matsunaga and K. Hayakawa, *Lancet Global Health*, 2018, **6**(9), e934.

16 (a) C. A. Nadgir and D. A. Biswas, *Cureus*, 2023, **15**, e38251; (b) M. A. Salam, M. Y. Al-Amin, M. T. Salam, J. S. Pawar, N. Akhter, A. A. Rabaan and M. A. A. Alqumber, *Healthcare*, 2023, **11**(13), 1946.

17 (a) A. M. Allahverdiyev, K. V. Kon, E. S. Abamor, M. Bagirova and M. Rafailovich, *Expert Rev. Anti-Infect. Ther.*, 2011, **9**, 1035; (b) J. He, K. Abdelraouf, K. R. Ledesma, D. S. L. Chow and V. H. Tam, *Int. J. Antimicrob. Agents*, 2013, **42**, 559; (c) E. Sans-Serramitjana, E. Fusté, B. Martínez-Garriga, A. Merlos, M. Pastor, J. L. Pedraz, A. Esquisabel, D. Bachiller, T. Vinuesa and M. Viñas, *J. Cystic Fibrosis*, 2016, **15**, 611.

18 (a) L. Boge, H. Bysell, L. Ringstad, D. Wennman, A. Umerska, V. Cassisa, J. Eriksson, M. L. Joly-Guillou, K. Edwards and M. Andersson, *Langmuir*, 2016, **32**, 4217; (b) L. Boge, K. L. Browning, R. Nordström, M. Campana, L. S. E. Damgaard, J. Seth Caous, M. Hellsing, L. Ringstad and M. Andersson, *ACS Appl. Mater. Interfaces*, 2019, **11**, 21314.

19 (a) D. Han, X. Liu and S. Wu, *Chem. Soc. Rev.*, 2022, **51**, 7138; (b) N. Kaur, P. Tiwari, K. S. Kapoor, A. K. Saini, V. Sharma and S. M. Mobin, *CrystEngComm*, 2020, **22**, 7513.

20 (a) C. Pettinari, R. Pettinari, C. Di Nicola, A. Tombesi, S. Scuri and F. Marchetti, *Coord. Chem. Rev.*, 2021, 214121; (b) R. Li, T. Chen and X. Pan, *ACS Nano*, 2021, **15**, 3808.

21 (a) D. F. Sava Gallis, K. S. Butler, J. O. Agola, C. J. Pearce and A. Mcbride, *ACS Appl. Mater. Interfaces*, 2019, **11**, 7782; (b) B. Soltani, H. Nabipour and N. A. Nasab, *J. Inorg. Organomet. Polym. Mater.*, 2018, **28**, 1090; (c) H. Nabipour, M. H. Sadr and G. R. Bardajee, *New J. Chem.*, 2017, **41**, 7364; (d) Z. Song, Y. Wu, Q. Cao, H. Wang, X. Wang and H. Han, *Adv. Funct. Mater.*, 2018, **28**, 1800011; (e) S. Kujur, A. Singh and C. Singh, *J. Aerosol Med. Pulm. Drug Delivery*, 2022, **35**, 259.

22 (a) S. W. Jaros, J. Krol, B. Bazanow, D. Poradowski, A. Chroszcz, D. S. Naestrov, A. M. Kirillov and P. Smolenski, *Molecules*, 2020, **25**, 2119; (b) W. Zhang, G. Ye, D. Liao, X. Chen, C. Lu, A. Nezamzadeh-Ejhieh, M. S. Khan, J. Liu, Y. Pan and Z. Dai, *Molecules*, 2022, **27**, 7166.

23 (a) C. Tamames-Tabar, E. Imbuluzqueta, N. Guillou, C. Serre, S. R. Miller, E. Elkaïm, P. Horcajada and

M. J. Blanco-Prieto, *CrystEngComm*, 2015, **17**, 456; (*b*) S. Quaresma, V. Andre, A. M. M. Antunes, S. M. Vilela, G. Amariei, A. Arenas-Vivo, R. Rosal, P. Horcajada and M. T. Duarte, *Cryst. Growth Des.*, 2020, **20**, 370.

24 F. Rafii, W. Franklin and C. E. Cerniglia, *Appl. Environ. Microbiol.*, 1990, **56**, 2146.

25 (*a*) D. Liu, D. Zou, H. Zhu and J. Zhang, *Small*, 2018, **14**, 1801454; (*b*) X. Chen and Q. Zhang, *Particuology*, 2019, **45**, 20; (*c*) L. Song, J. Zhang, L. Sun, F. Xu, F. Li, H. Zhang, X. Si, C. Jiao, Z. Li, S. Liu, Y. Liu, H. Zhou, D. Sun, Y. Du, Z. Cao and Z. Gabelica, *Energy Environ. Sci.*, 2012, **5**, 7508.

26 D. J. Levine, T. Runčevski, M. T. Kapelewski, B. K. Keitz, J. Oktawiec, D. A. Reed, J. A. Mason, H. Z. H. Jiang, K. A. Colwell, C. M. Legendre, S. A. FitzGerald and J. R. Long, *J. Am. Chem. Soc.*, 2016, **138**, 10143.

27 A. Boultif and D. Loueer, *J. Appl. Crystallogr.*, 1991, **24**(pt 6), 987.

28 W. I. F. David, K. Shankland, J. Van De Streek, E. Pidcock, W. D. S. Motherwell and J. C. Cole, *J. Appl. Crystallogr.*, 2006, **39**, 910.

29 B. H. Toby and R. B. Von Dreele, *J. Appl. Crystallogr.*, 2013, **46**, 544.

30 P. Giannozzi, S. Baroni, N. Bonini, M. Calandra, R. Car, C. Cavazzoni, D. Ceresoli, G. L. Chiarotti, M. Cococcioni and I. Dabo, *J. Phys.: Condens. Matter*, 2009, **21**, 395502.

31 N. A. Khan, N. Kaur, P. Owens, O. P. Thomas and A. Boyd, *Int. J. Mol. Sci.*, 2022, **23**, 1991.

32 R. Novick, *Virology*, 1967, **33**, 155.

33 (*a*) P. Sheth, S. W. Stein and P. B. Myrdal, *AAPS PharmSciTech*, 2014, **16**, 192; (*b*) Y. Zheng, Y. Zhao, M. Bai, H. Gu and X. Li, *J. Mater. Chem. B*, 2022, **10**, 5666.

34 A. A. Voskanyan, V. G. Goncharov, N. Novendra, X. Guo and A. Navrotsky, *ACS Omega*, 2020, **5**, 13158.

35 A. Shariati, M. Arshadi, M. A. Khosrojerdi, M. Abedinzadeh, M. Ganjalishadi, A. Maleki, M. Heidary and S. Khoshnood, *Front. Public Health*, 2022, **10**, 1025633.

36 J. E. Mondloch, O. Karagiaridi, O. K. Farha and J. T. Hupp, *CrystEngComm*, 2013, **15**, 9258.

37 S. Chakraborty, T. Gruber, C. E. Barry, H. I. Boshoff and K. Y. Rhee, *Science*, 2013, **339**, 88.